

## Turbulence Measurements from Compliant Moorings. Part I: Motion Characterization

SAMUEL HARDING

*Pacific Northwest National Laboratory, Richland, Washington*

LEVI KILCHER

*National Renewable Energy Laboratory, Golden, Colorado*

JIM THOMSON

*Applied Physics Laboratory, University of Washington, Seattle, Washington*

(Manuscript received 30 September 2016, in final form 10 February 2017)

### ABSTRACT

High-fidelity measurements of turbulence in the ocean have long been challenging to collect, in particular in the middle of the water column. In response, a measurement technique has been developed to deploy an acoustic Doppler velocimeter (ADV) to midwater locations on a compliant mooring. A variety of instrumentation platforms have been deployed as part of this work with a range of dynamic motion characteristics. The platforms discussed herein include the streamlined StableMoor buoy (SMB), the Tidal Turbulence Mooring (TTM) system based on a conventional 0.9-m spherical buoy, and a 100-lb sounding weight suspended from the stern of a research vessel. The ADV head motion is computed from inertial motion sensors integrated into an ADV, and the spectra of these signals are investigated to quantify the motion of each platform. The SMB with a single ADV head mounted on the nose provided the most stable platform for the measurement of tidal turbulence in the inertial subrange for flow speeds exceeding  $1.0 \text{ m s}^{-1}$ . The modification of the SMB with a transverse wing configuration for multiple ADVs showed a similar frequency response to the nose configuration in the horizontal plane but with large contamination in the vertical direction as a result of platform roll. While the ADV motion on the TTM was significant in the horizontal directions, the vertical motion of this configuration was the most stable of all configurations tested. The sounding weight measurements showed the greatest motion at the ADV head but are likely to be influenced by both prop-wash and vessel motion.


### 1. Introduction

The measurement of turbulence in energetic ocean currents represents a long-standing practical challenge in ocean engineering. The understanding of midwater oceanic turbulence is required in a wide range of fields, including marine microbiology, ecology, mooring technologies, mixing, and model validation. Though the mean kinetic energy and bulk turbulence statistics of

tidal currents can be characterized with relative ease using acoustic Doppler current profilers (ADCPs) (Guerra París and Thomson 2017), the higher temporal and spatial resolution required to detect the full range of turbulent scales poses a greater measurement challenge.

Oceanographic properties have been successfully measured from moored platforms through the measurement and removal of the platform motion. Such motion-correction processes have been used in the characterization of turbulent tidal flow velocities (Kilcher et al. 2014; Thomson et al. 2013, 2014) and thermal variation dissipation rates (Moum and Nash 2009; Perlin and Moum 2012). In this process, the motion of the submerged instrumentation platforms can be measured using a combination of acceleration, angular rotation rate, compass, and pressure sensor data. Integrated

---

 Denotes content that is immediately available upon publication as open access.

---

Corresponding author: Samuel Harding, samuel.harding@pnnl.gov

multiaxis inertial measurement units (IMUs) are available to detect both the linear acceleration and the angular rotation rate in pitch, roll, and yaw.

One application of tidal current research of increasing interest is in the harnessing of energetic flows for electricity generation. For this application, the understanding of the high-fidelity flow velocities is critical to the design and operation of a tidal energy conversion device and model validation (Afgan et al. 2013; Milne et al. 2015).

High-frequency point velocity measurements can be used to directly characterize many key properties of tidal turbulence. This is most widely achieved in the field through the use of an acoustic Doppler velocimeter (ADV). These instruments operate by ensonifying a volume of fluid with a known acoustic signal. In the case of the Nortek Vector ADV used in these experiments, the frequency shift in the reflected acoustic signal is measured by receivers in a bistatic configuration to infer three components of velocity with relatively high temporal resolution (Kraus et al. 1994; Nortek AS 2005).

The challenge with deploying a point-measurement velocimeter is accessing the areas of interest in the water column. Large hydrodynamic loads and moments are generated on structures that are fixed to the ocean floor or penetrate from the surface. These moments can be mitigated through the use of compliant mooring lines to submerged instrumentation. With the removal of fixed structures under moored configurations, the motion of the instrument relative to the motion of the water can become significant (Thomson et al. 2013; Paskyabi and Fer 2013; Matt et al. 2014).

This paper presents the experimental campaign and subsequent data analysis used to characterize the motion of an ADV mounted on a range of subsea platform geometries and configurations. The primary aim of this study is to identify the predominant contaminating frequencies and modes of platform motion. Using the same dataset, the motion correction of the measured velocity signals is presented in the companion paper (Kilcher et al. 2017, hereafter Part II). Persistent signal contamination of ADV velocity measurements is observed when the ADV head velocity is large. The motion contamination can thus be minimized through the selection of the most stable platform from which to deploy the ADV, as discussed in Part II. In short, the best form of motion correction is motion prevention. This work compares the motion of different platforms in order to inform the reader interested in deploying similar systems.

To begin, the instrumentation and mooring hardware used in this study are introduced. The coordinate system

used in the analysis is then explained and justified. The motion of the ADV is then described for all deployed platform geometries and configurations, with the key motion dynamics identified and explained. The analysis concludes with a direct comparison of the ADV head motion characteristics between all platform configurations in flows with a mean speed of  $1\text{--}2\text{ m s}^{-1}$ .

All measurements used in this work were acquired in Admiralty Inlet, Washington, which connects the Puget Sound to the Strait of Juan de Fuca. The specific deployment site was approximately 500 m west-southwest of Admiralty Head at  $48.153^{\circ}\text{N}$ ,  $122.678^{\circ}\text{W}$ . The site has a large semidiurnal tidal flow with a mean water depth of approximately 60 m. Additional site details can be found in Part II, and are described in detail by Thomson et al. (2012) and Polagye and Thomson (2013).

## 2. Instrumentation

### a. Inertial measurement units

The IMU used in the following experiments is the nine-axis LORD MicroStrain 3DM-GX3-25-OEM inertial sensor (LORD MicroStrain 2014). This IMU incorporates a triaxial accelerometer, a triaxial gyroscope, and a triaxial magnetometer to measure static and dynamic orientation and inertial measurements. This unit is an industrial-grade attitude heading and reference system (AHRS) with integrated magnetometers, with a form factor of  $38 \times 24 \times 12\text{ mm}$ . The IMU was integrated into the Nortek Vector ADVs with tight time synchronization, with the unit axes orthogonal to the axes of the ADV pressure case.

### b. Mooring hardware

The three instrumentation platforms considered in this motion comparison analysis are introduced below. A schematic of all three platforms is shown in Fig. 1 with key parameters summarized in Table 1.

#### 1) STABLEMOOR BUOY PLATFORM

The streamlined StableMoor buoy (SMB) is an instrumentation platform produced by DeepWater Buoyancy, Inc. (formerly designed by Flotation Technologies). The buoy is manufactured using syntactic foam with a protective glass-reinforced plastic (GRP) shell. The elongated form of the buoy and GRP tail vane are designed to reduce drag loads and to increase dynamic stability in energetic flow conditions. However, the disadvantages of this design include the significant cost and the relatively large size of the platform, which make deployment and retrieval more challenging.

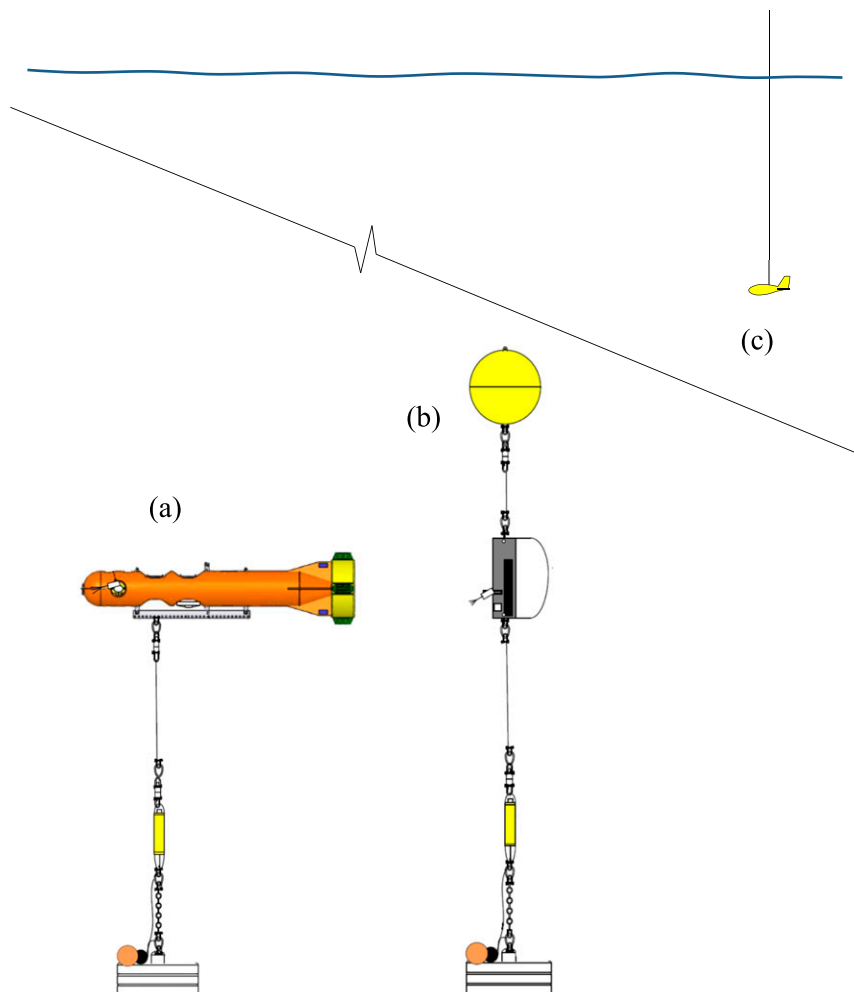


FIG. 1. Platform schematics: (a) SMB, (b) TTM, and (c) sounding weight tethered to the research vessel.

In this study, ADVs were mounted to the SMB in two configurations, both with the ADV head in the upward-looking direction:

- **Winged mode:** A carbon-fiber beam with an elliptical cross section was installed near the nose of the SMB with a port and starboard ADV attached to either end, as shown in Fig. 2a. The ADV bodies were installed in the instrumentation wells in the SMB body.
- **Nose mode:** The carbon-fiber beam was removed and a single ADV was installed, with the ADV head attachment protruding from the nose of the SMB, as shown in Fig. 2b.

A 1200-kHz RD Instruments (RDI) Workhorse Sentinel was also installed in a down-looking orientation in an instrument well on the SMB. This unit was configured to measure the water profile from the platform to the seabed as well as the bottom-track (BT) velocity. A

comparison of the BT velocity measured by this instrument and the IMU method is discussed in the appendix.

## 2) TIDAL TURBULENCE MOORING PLATFORM

The Tidal Turbulence Mooring (TTM) system consists of two ADVs mounted to a vane that is then fixed to a mooring line between an anchor on the seabed and a 0.9-m spherical buoy. This is the same configuration as used in previous experiments by Thomson et al. (2013). The principal components of the TTM are shown in Fig. 3.

## 3) SOUNDING WEIGHT PLATFORM

The sounding weight used in these experiments is a streamlined instrumentation platform suspended below the research vessel. The 100-lb USGS “Columbus type” weight is cast from lead, with aluminum tail

TABLE 1. Velocimetry platform properties.

Platform	Fastening location	Streamwise platform length (m)	Line length $L$ (m)	Dry mass $m$ (kg)	Submerged mass <sup>a</sup> (kg)
SMB	Seabed	3.6	9.5	295	-185
TTM	Seabed	0.9	11	137	-320
Sounding weight	Vessel	0.4	20, 30, 40	45	41

<sup>a</sup> Negative values indicate net buoyancy.

fins. A davit was used to deploy the sounding weight over the port side of the vessel (Fig. 4a), and an A-frame winch was used for simultaneous deployments from the aft of the vessel. The sounding weight represents a relatively compact, inexpensive platform with flexibility to be rapidly deployed and retrieved or even moved to perform spatial transects. The cabled ADV head was installed in an upward-looking orientation at the nose of the sounding weight, as shown in Fig. 4b.

The sounding weights were deployed from the research vessel in two separate experiments. In the first, both the port and aft sounding weights were deployed with a submerged line length of 20 m. In the second, the line lengths of the port and aft sounding weights were set at 30 and 40 m, respectively.

### 3. Coordinate system

Velocity measurements are discussed throughout this study in terms of two stationary coordinate systems: 1) the “Earth frame” is the coordinate system in which motion measurement is performed and 2) the local “analysis frame” is the coordinate

system in which the platform motion is analyzed and discussed.

For more details on the reference frames used in the motion characterization process, refer to Kilcher et al. (2016). Open-source Python tools for calculating ADV head velocities using ADV-IMU data are available online (at <http://lkilcher.github.io/dolfyn/>).

#### a. The Earth frame

The Earth coordinate system is the coordinate system in which the orientation of the ADV is measured and is the coordinate system in which motion correction is calculated. This work utilizes “ $e$ ” superscripts to denote an east, north, up (ENU) Earth coordinate system with basis vectors of  $\hat{x}^e$ ,  $\hat{y}^e$ , and  $\hat{z}^e$ , respectively.

The motion of the ADV head can be considered as the summation of two components—the linear motion component  $\mathbf{u}_a^e(t)$  and the rotational motion component  $\mathbf{u}_\omega^e(t)$ —such that  $\mathbf{u}^e(t) = \mathbf{u}_a^e(t) + \mathbf{u}_\omega^e(t)$ .

The linear motion component is defined mathematically by Eq. (1). Here  $\mathbf{u}_a^e(t)$  is the IMU-measured acceleration signal in the Earth frame and  $\{\cdot\}_{HP(f_a)}$  denotes a high-pass filter of frequency  $f_a$ . The acceleration must be high-pass filtered in this way to remove the

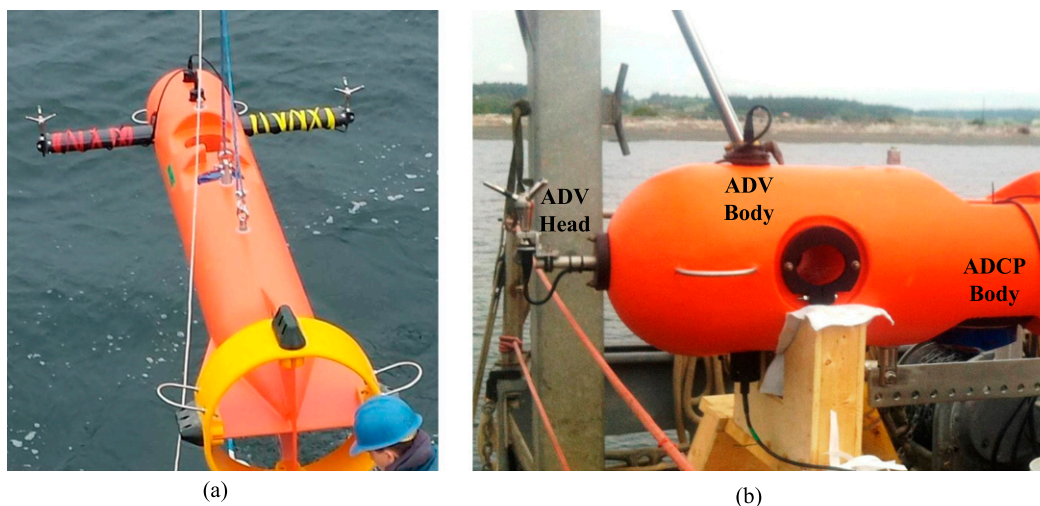


FIG. 2. SMB mooring configurations: (a) two ADVs in winged mode and (b) a single ADV in nose mode.

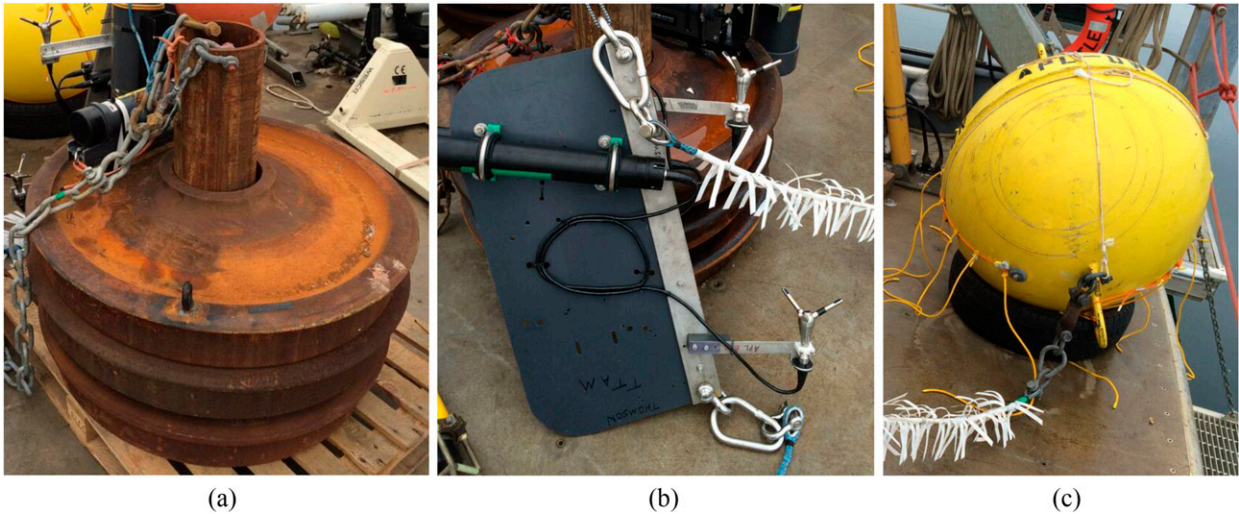


FIG. 3. TTM components: (a) seabed anchor constructed using three railroad wheels, (b) two ADVs on strong-back vane attached to mooring line, and (c) spherical buoy at end of mooring line.

influence of gravity and low-frequency bias (bias drift), which are inherent to IMU acceleration measurements,

$$\mathbf{u}_a^e(t) = \int \{\mathbf{a}^e(t)\}_{\text{HP}(f_a)} dt. \quad (1)$$

Bench tests of the Microstrain IMU indicate that accelerometer drift is strongest at frequencies less than 0.01 Hz. Therefore, in order to remove bias drifts, which cause large errors in  $\mathbf{u}_a^e$ , the measured  $\mathbf{a}^e$  has been high-pass filtered with a threshold of  $f_a = 0.033$  Hz (Part II). As a result, real motions at and below  $f_a$  will be underestimated using the ADV-IMU method.

The second component,  $\mathbf{u}_\omega^e(t)$ , is due to rotational motion of the ADV head about the IMU and is defined mathematically by

$$\mathbf{u}_\omega^e(t) = \mathbf{R}^T(t)[\boldsymbol{\omega}^*(t) \times \mathbf{I}^*]. \quad (2)$$

Here  $\boldsymbol{\omega}^*$  is the IMU-measured rotation rate,  $\mathbf{I}^*$  is the vector from the IMU to the ADV head,  $\times$  indicates a cross product, and superscript  $*$  denotes a quantity in the “ADV body” coordinate system. This coordinate system is used explicitly here to emphasize that  $\mathbf{I}^*$  is constant in time. The transformation matrix of  $\mathbf{R}$  describes the orientation of the ADV body in the Earth coordinate frame.

*b. The analysis frame*

The fixed reference frame used in this analysis is based on the principal flow direction of the tidal current, where  $\hat{\mathbf{x}}$  denoted the “streamwise” direction,  $\hat{\mathbf{y}}$  is the “cross stream” direction (defined by the right-hand rule relative to  $\hat{\mathbf{x}}$  and  $\hat{\mathbf{z}}$ ), and  $\hat{\mathbf{z}}$  is the “vertical up” direction. Note that throughout this work, vector quantities with no superscript

are in this stationary frame. The orientation of this frame relative to the Earth frame is defined by Eq. (3), where  $\theta$  is the clockwise angle from east to the streamwise direction,

$$\begin{bmatrix} \hat{\mathbf{x}} \\ \hat{\mathbf{y}} \\ \hat{\mathbf{z}} \end{bmatrix} = \begin{bmatrix} \cos(\theta) & \sin(\theta) & 0 \\ -\sin(\theta) & \cos(\theta) & 0 \\ 0 & 0 & 1 \end{bmatrix} \begin{bmatrix} \hat{\mathbf{x}}^e \\ \hat{\mathbf{y}}^e \\ \hat{\mathbf{z}}^e \end{bmatrix}. \quad (3)$$

The principal flow direction is often calculated using the entirety of the velocity data available for a site in order to characterize the “tidal average” principal flow direction  $\theta_{\text{tide}}$ . However, characterizing the platform motion in this reference frame caused cross contamination between the motion signal in the streamwise and cross-flow directions at this site. This is because the mean flow direction of each 128-s data ensemble used in the motion characterization deviated from the tidal-average principal flow direction as shown in Fig. 5a. Some level of directional asymmetry is often observed in tidal flows (Polagye and Thomson 2013), and for this reason the principal flow direction was calculated for each 128-s ensemble of data analyzed. Denoting this direction as  $\theta$ , the difference between the tidal-average principal direction and the 128-s ensemble-averaged principal direction,  $\Delta\theta = \theta - \theta_{\text{tide}}$ , is shown in Fig. 5b.

**4. Frequency response of ADV motion**

The velocity of the ADV head resulting from platform motion is presented herein in the frequency domain in the same way as TKE spectra are often presented for turbulent flows. Specifically, spectra are calculated

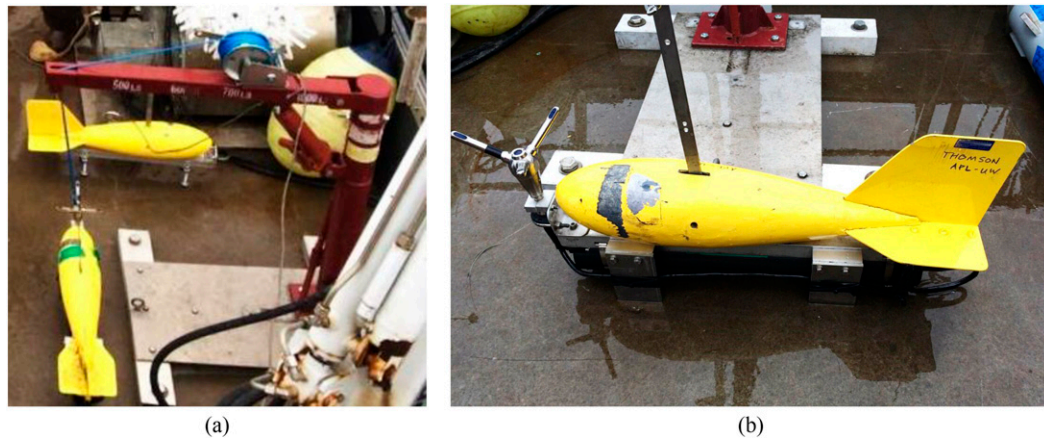


FIG. 4. Sounding weight platform: (a) sounding weight tethered to davit for vessel-mounted deployment and (b) ADV head configuration.

using a fast Fourier transform ( $\mathcal{F}$ ) of the ADV head velocity using 128 s of detrended Hanning-windowed segments with 50% overlap such that  $S\{u\}(f) = |\mathcal{F}\{u\}|^2$ . Spectra are normalized to preserve variance such that  $\int S\{u\} df = \overline{u^2}$ .

The energy spectra of the ADV head velocity in the direction of the streamwise, transverse, and vertical directions of the 128-s ensemble averaged principal coordinate system are denoted as  $S\{u\}$ ,  $S\{v\}$ , and  $S\{w\}$ , respectively.

The integration of the IMU acceleration signal to calculate the linear motion component [Eq. (1)] increases the bias-drift noise at low frequencies. However, the high-pass filtering reduces this noise so that it does not contaminate motion correction above the filter threshold frequency of 0.033 Hz. As such the error in the ADV head velocity resulting from the measured acceleration components is frequency dependent. Conversely, the measurement error in the rotation-induced ADV head velocity propagates linearly with the error in the rotation

rate measurement [Eq. (2)] and is constant over all frequency bands.

The velocity error components resulting from sensor error were measured experimentally by mounting the IMU on a fixed test bench and acquiring the motion data. The spectra of the velocity error in the linear motion component of the ADV was observed to have a peak at the filter threshold frequency (0.033 Hz) of  $10^{-3} \text{ m}^2 \text{ s}^{-2} \text{ Hz}^{-1}$  in the horizontal direction and  $10^{-5} \text{ m}^2 \text{ s}^{-2} \text{ Hz}^{-1}$  in the vertical direction, reducing with increased frequencies at a rate of  $f^{-2}$ . The velocity error in the rotation-induced velocity was observed to be a constant  $10^{-7} \text{ m}^2 \text{ s}^{-2} \text{ Hz}^{-1}$  in all frequency bands. For further discussion on the relative contribution of this error to motion-correction techniques, refer to Part II.

#### a. StableMoor buoy

The energy spectra of the ADV motion are presented in Fig. 6 for the two ADV configurations tested—winged mode and nose mode. This figure presents the mean

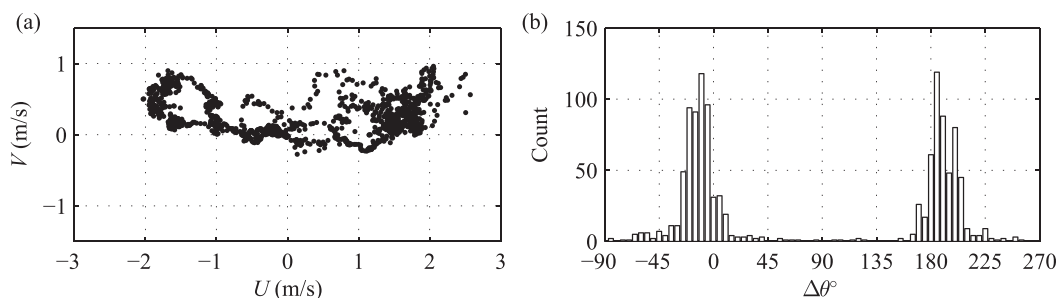


FIG. 5. Representative flow velocities at deployment site using SMB winged deployment data showing (a) scatterplot of ensembles of velocity data averaged over 128 s on the tidal-average principal coordinate system and (b) the difference in angle between the tidal-average principal direction and the 128-s ensemble-averaged principal direction (with  $+\Delta\theta$  defined as clockwise from the  $U$  direction).

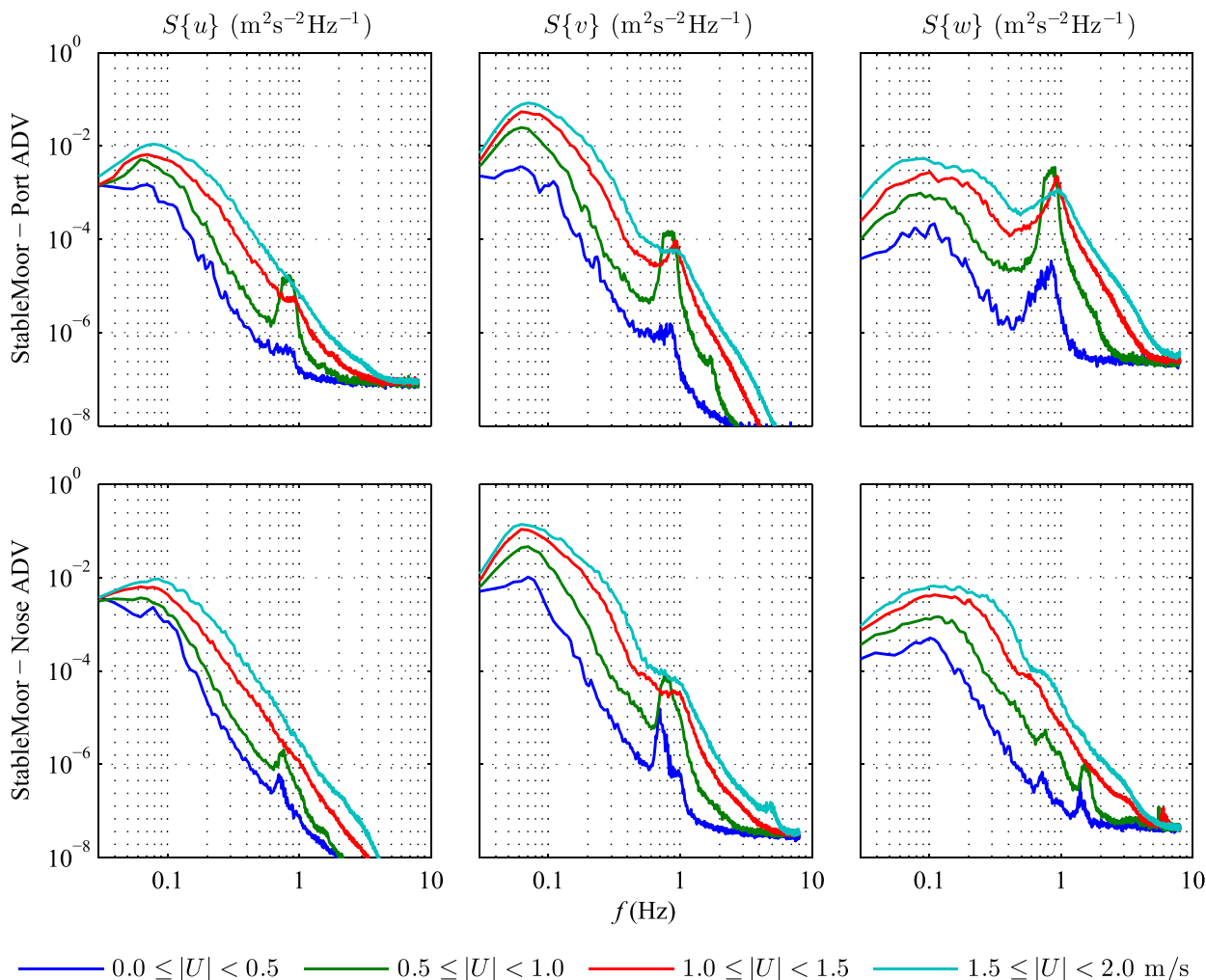


FIG. 6. ADV head velocity spectra for SMB deployments in (top) winged mode and (bottom) nose mode, where  $u$  is aligned with the principal flow direction for the 128-s ensemble,  $v$  is the cross-flow direction, and  $w$  is the vertical direction for four different values of  $U$  presented in different colors.

velocity spectra in terms of mean flow velocity  $U$  using  $0.5 \text{ m s}^{-1}$  bins. Only the port ADV results are shown in this figure, as these are representative of both the port and starboard ADV motions in winged mode. In general, the motion of the instrument increases at higher mean flow velocities.

The energy spectra of the ADV head velocity for the port instrument in winged mode (represented by the top plot in Fig. 6) show the majority of the motion energy in the frequency range of 0.07–0.2 Hz. In the lower limits of the frequency range ( $f \leq 0.3 \text{ Hz}$ ), the motion is predominantly in the lateral direction. The peak energy spectra of the ADV head velocity in the cross-flow direction is  $S\{v\}(0.07 \text{ Hz}) \approx 0.1 \text{ m}^2 \text{ s}^{-2} \text{ Hz}^{-1}$ .

A natural frequency phenomenon is observed at 0.8 Hz in the transverse and vertical directions, with a maximum response in the  $0.5 < U \leq 1.0 \text{ m s}^{-1}$  velocity

band. The frequency response was calculated for the mean velocity range where the high-frequency resonance was observed,  $0 < U \leq 1.0 \text{ m s}^{-1}$ . Figure 7 shows the key dynamics of the SMB motion for the winged configuration (port ADV) and nose configuration.

The higher-frequency resonance is observed in the frequency response for the transverse motion and also observed in vertical direction in winged mode. The motion can be visualized as a “swimming” dynamic, where the platform yaws about the vertical axis with an accompanying oscillating translation in the lateral direction. As the SMB moves in the lateral direction, the mooring line fastened to the underside of the buoy causes a rolling motion at the same frequency. In the case of the winged configuration, the angular velocity of the roll is translated into a vertical motion of the ADV heads, which are mounted on a horizontal moment

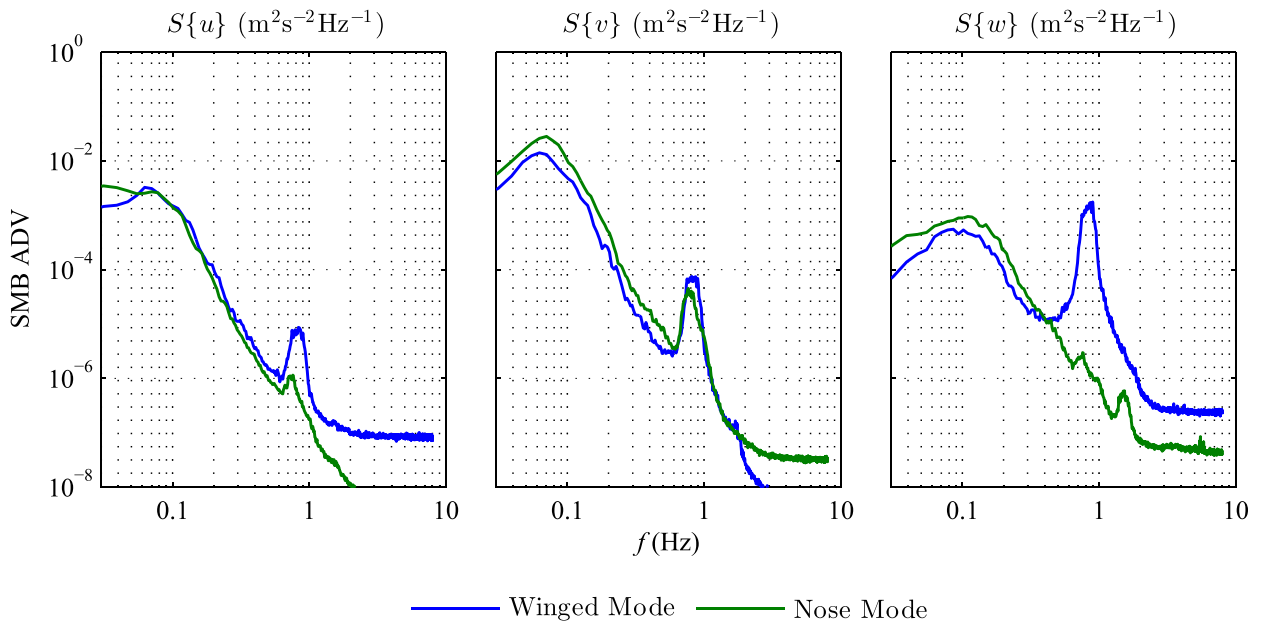


FIG. 7. Motion spectra of SMB ADV for velocity range  $0 \leq U < 1 \text{ m s}^{-1}$  for starboard ADV in winged mode (blue) and nose ADV (green), where  $u$  is aligned with the principal flow direction for the 128-s ensemble,  $v$  is the cross-flow direction, and  $w$  is the vertical direction.

arm. This introduces a strong rotation-induced vertical velocity at the same frequency as the lateral motion, at  $f = 0.8 \text{ Hz}$ , as shown in Fig. 8.

### b. Tidal Turbulence Mooring

The ADV head velocity in the TTM configuration is a function of two dynamic phenomena. First, the motion of the spherical buoy dominates the motion of the system at the natural frequency of the pendular system. The ability of the ADV mounting board to yaw about the mooring line also introduces a lateral motion of the ADV head. The frequency response of the ADV head motion of the TTM system is presented in Fig. 9.

The dominant motion of the system, particularly at low flow speeds, was seen in the transverse direction and results from the vortex-induced velocity (VIV) of the large spherical mooring buoy at the end of the mooring line (Fig. 3c). This configuration can be interpreted as a buoyant pendulum system, with a natural frequency described as a function of the Strouhal number of the spherical buoy  $St$  by

$$f_n = \frac{U \times St}{D}. \quad (4)$$

After verifying that the drag force may be neglected, the Strouhal number can be approximated to account for added mass by using Eq. (5) (Williamson and Govardhan 1997; Govardhan and Williamson 2005). Here  $Fr = U/(gD)^{1/2}$ ,  $m^*$  is the sphere mass normalized by the displaced mass of fluid [ $m^* = m/(1/6)\pi D^3 \rho$ ],  $L$  is

the mooring line length, and  $C_a$  is the added mass coefficient equal to 0.5,

$$St \approx \frac{1}{2\pi Fr \sqrt{L/D}} \sqrt{\frac{1 - m^*}{C_a + m^*}}. \quad (5)$$

By substituting Eq. (5) into Eq. (4), the theoretical natural frequency of the buoyant spherical pendulum is calculated as 0.13 Hz. The peak motion frequencies measured in the lateral direction are in the range of 0.10 – 0.25 Hz. The comparable frequencies of this motion are interpreted as confirmation of the a priori assumption of vortex-induced motion of the spherical buoy.

The higher-frequency ADV head velocities measured in the lateral direction are attributed to the ability of the ADV vane to yaw about the mooring line in a fluttering motion. As such, the amplitude of the cross-flow motion at this frequency is larger than the streamwise and vertical motion components. Evidence of motion in these directions at the same frequency is due to the mooring line deviating from vertical due to blowdown of the TTM system to an angle of  $20^\circ$  at mean flow speeds of  $2.0 \text{ m s}^{-1}$  (Thomson et al. 2013).

### c. Sounding weight

The frequency response amplitude of the sounding weight ADV velocity is presented in Fig. 10. The sounding weight was deployed from the research vessel as it was holding station in flow speeds of  $1.0 < U \leq 1.5 \text{ m s}^{-1}$ . The



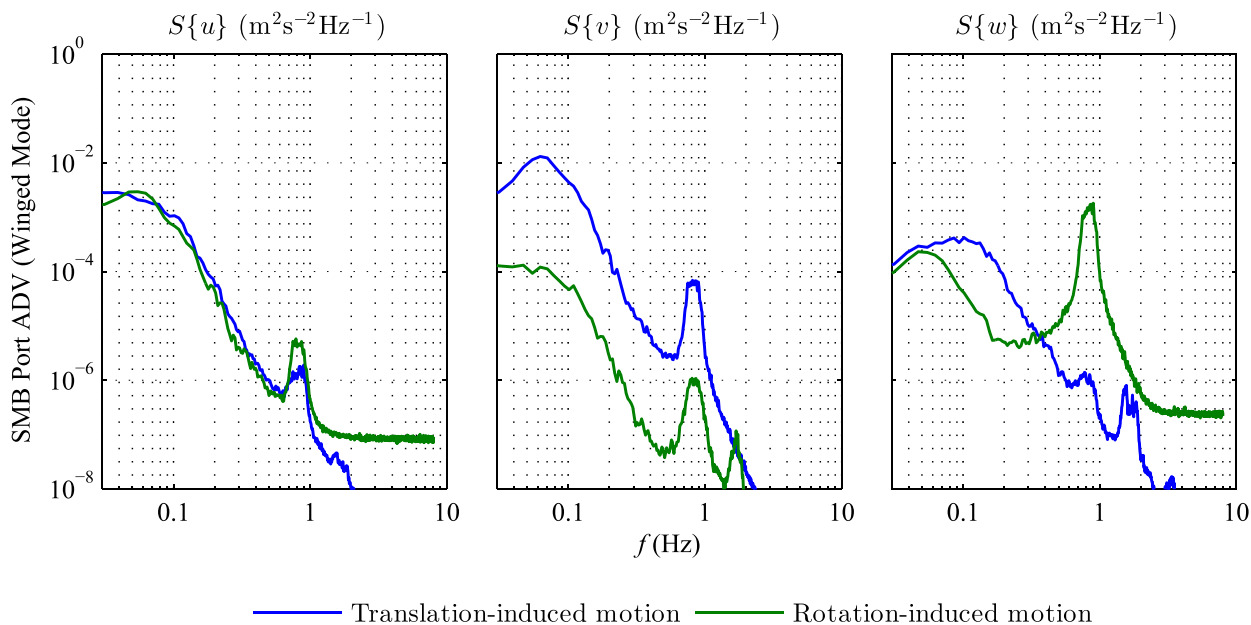


FIG. 8. Comparison of contribution of platform translation and rotation to ADV velocity spectra for SMB deployments in winged mode for velocity range  $0 \leq U < 1 \text{ m s}^{-1}$ , where  $u$  is aligned with the principal flow direction for the 128-s ensemble,  $v$  is the cross-flow direction, and  $w$  is the vertical direction.

port deployments used the davit for deployment with a 3/16-in.-diameter line. The aft deployments utilized the A-frame winch, with a 9/16-in.-diameter tethering line.

A significant motion of the sounding weight is a pitching–heaving dynamic at a frequency of  $f \approx 0.27 \text{ Hz}$ . The amplitude of this motion is significantly greater during the first deployment of the sounding weights,

which used 20-m line lengths for both the port- and aft-mounted platforms.

The motion of the sounding weight is subject to forcing terms not found in the SMB and TTM. First, the instrument is tethered to the research vessel, which is holding station in the unsteady flows and is affected by surface dynamics (waves and swell). This introduced an

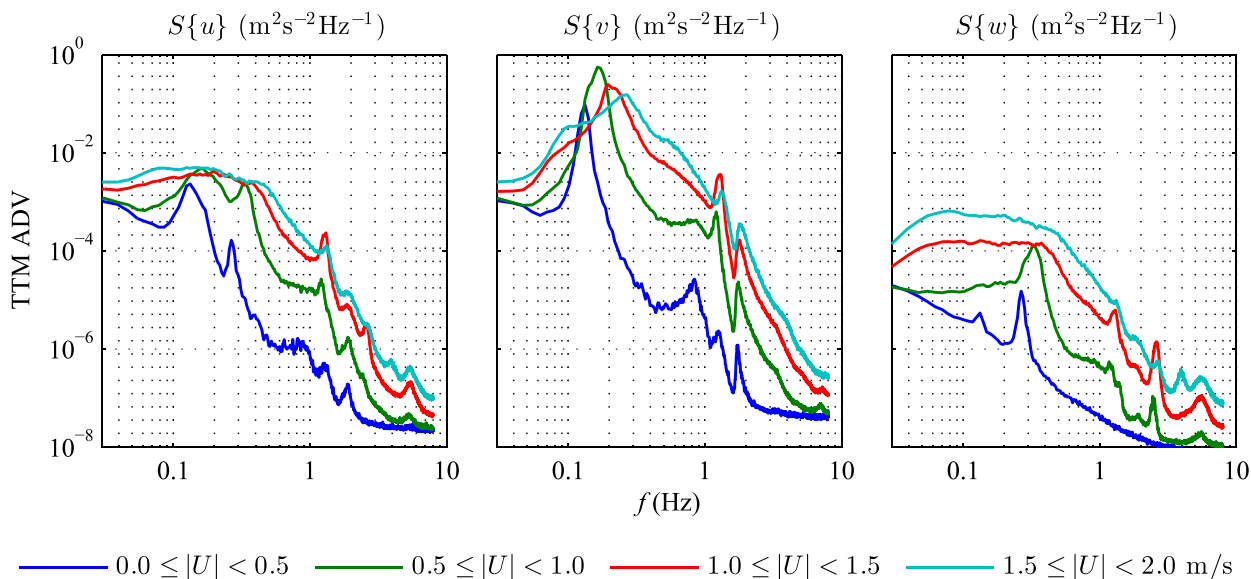


FIG. 9. Motion spectra of TTM ADV for four different values of  $U$  presented in different colors, where  $u$  is aligned with the principal flow direction for the 128-s ensemble,  $v$  is the cross-flow direction, and  $w$  is the vertical direction.

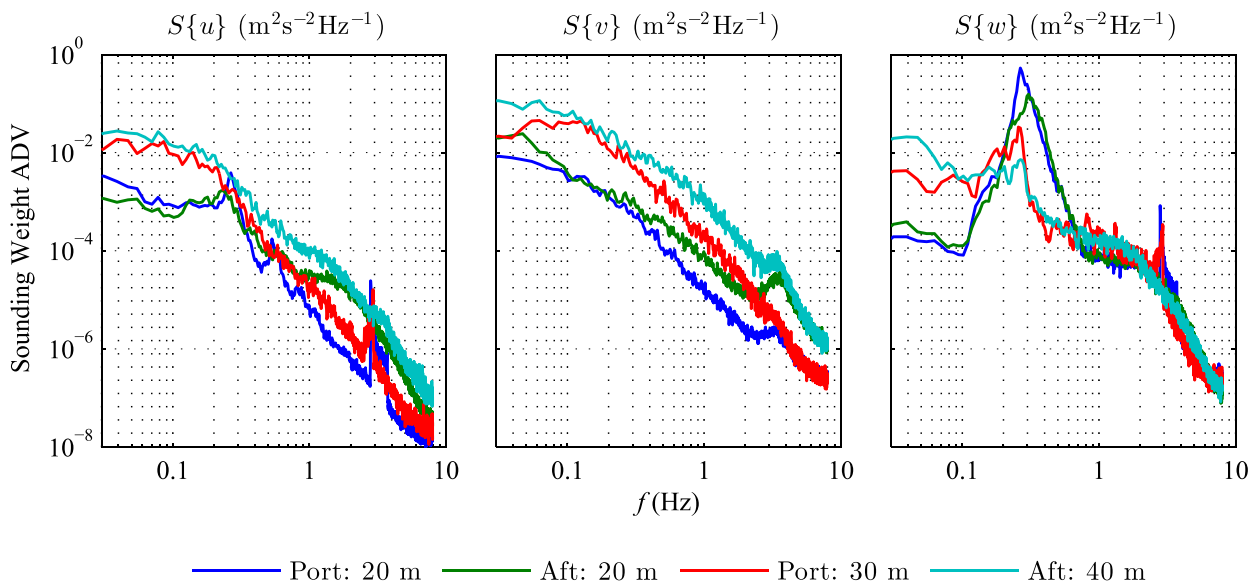


FIG. 10. Motion spectra of sounding weight ADV for 20, 30, and 40 m ranges of tethering lines and port and aft vessel deployment locations, where  $u$  is aligned with the principal flow direction for the 128-s ensemble,  $v$  is the cross-flow direction, and  $w$  is the vertical direction.

additional velocity source not found in the seabed-tethered systems. The authors expect that the vessel roll motion may be the cause of this significant vertical motion component of the sounding weight, with the conditions during the 20-m deployment generating more vessel motion than the 30- to 40-m deployment. This explains the increased motion of the port-mounted platforms relative to the aft-mounted platforms.

As a result of this deployment method, the ADV may also be exposed to the prop-wash aft of the propellers, which is particularly significant for the shorter tethering lines and the instrument deployed from the aft rather than the port. The deployment of each sounding weight was limited to between 30 and 60 min at a limited velocity range, so the frequency response of Fig. 10 represents significantly less data than the SMB and TTM deployments. The combination of these factors makes direct comparison of the sounding weight with the SMB and TTM deployments difficult. While strumming was observed in the lines above the water level, the frequency of this exceeds that captured by the ADV-IMU and the resulting ADV head velocity is expected to be negligible.

## 5. Platform motion comparison

The ADV head motion of a range of platform configurations discussed herein is presented in Fig. 11. These spectra represent the ADV head velocity for flow

conditions in the range of  $1.0 < U \leq 2.0 \text{ m s}^{-1}$  as the velocity range most relevant to energetic tidal current applications.

In the streamwise direction, the SMB platform is significantly more stable than the TTM at  $f > 0.1 \text{ Hz}$ , with an order of magnitude reduction in motion-induced velocities for  $f > 0.1 \text{ Hz}$ . This high-frequency stability is comparable in the transverse direction. Though there is evidence of the SMB natural frequency in the cross-flow direction at  $f \approx 0.8 \text{ Hz}$ , the ADV head velocities remain significantly lower than the TTM platform. This is particularly significant in the context of turbulence measurements that utilize the higher-frequency capabilities of the ADV to characterize the inertial subrange.

The TTM is at least as stable as the SMB and sounding weight at lower frequencies ( $f < 0.1 \text{ Hz}$ ) in all directions. However, at frequencies above the threshold, the TTM ADV velocity in the streamwise and lateral directions is comparable to that of the sounding weight and significantly more than the SMB. In particular, the VIV frequency of the spherical buoy causes a peak in the cross-flow motion of the TTM at  $f \approx 0.13 \text{ Hz}$ .

However, the TTM is the most stable platform at all frequencies in the vertical direction. This is particularly important in the use of ADVs to characterize turbulence, because the vertical component of velocity is the cleanest measurement from the ADV head in the configurations deployed as a result of the beam

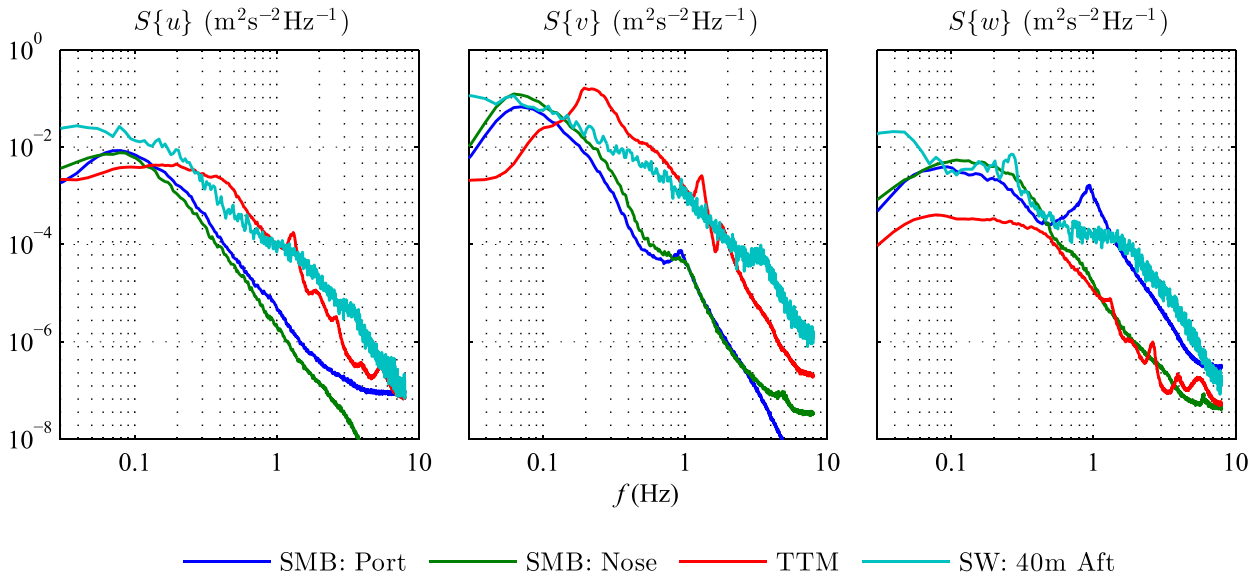


FIG. 11. ADV head velocity spectra for SMB, TTM, and SW instrumentation platforms and port-aft configurations, where  $u$  is aligned with the principal flow direction for the 128-s ensemble,  $v$  is the cross-flow direction, and  $w$  is the vertical direction.

geometry. As a result, for isotropic turbulence, this velocity component provides the best estimate of TKE dissipation rate via the inertial subrange. The TTM is therefore the most appropriate mooring for this use, though its performance is inferior compared to the SMB in the other directions of motion.

### 6. Conclusions

Tethered instrumentation platforms are able to be used to deploy ADVs in energetic tidal environments. However, large motion-induced velocities at the ADV head can result in persistent motion contamination of the corrected velocity signal. The platform motions analyzed show that the frequency response is sensitive to the flow speed and the platform geometries and configurations.

To summarize, the SMB with a single ADV deployed on the nose provided the most stable ADV measurement, with superior frequency response at  $f < 0.1$  Hz. This resulted in an uncontaminated motion-corrected measurement of the velocity spectra throughout the inertial subrange of the turbulence measurement. When the SMB was deployed in wing mode, the roll of the platform induced a significant vertical velocity component at the ADV head at  $f \approx 0.8$  Hz. While providing a stable platform at relatively low frequencies ( $f < 0.1$  Hz) and all frequencies in the vertical direction, the motion at the TTM ADV was an order of magnitude larger than that of the SMB in the streamwise and transverse directions for most of

the frequencies corresponding to the inertial subrange turbulence at the deployment site.

The very low ADV head motion in the vertical direction when mounted on the TTM is significant, as this corresponds to the direction of the lowest velocity signal noise when the ADV head is mounted in the upward-looking configuration. This combination of low platform motion and instrument noise identifies this configuration as the most appropriate for estimating TKE dissipation rates in the inertial subrange. The TTM also has the advantage of being significantly less expensive than either of the SMB configurations presented.

The performance of the sounding weight platform showed a very large oscillatory component in the vertical direction for the 20-m deployments as the platform became unsteady in pitch. For the case of the sounding weight, the induced motion is a function of both the platform dynamics and the vessel motion to which it is coupled. The resulting motion contamination is the largest for all the platforms considered in these tests over most of the frequency range considered.

*Acknowledgments.* The authors thank Joe Talbert and Alex de Klerk for the fabrication and preparation of the moorings, as well as the engineering support during the field operations. The authors thank Capt. Andy Reay-Ellers for his assistance in the precise deployment and retrieval of mooring hardware. This research was supported by the U.S. Department of Energy’s Office of Energy Efficiency and Renewable

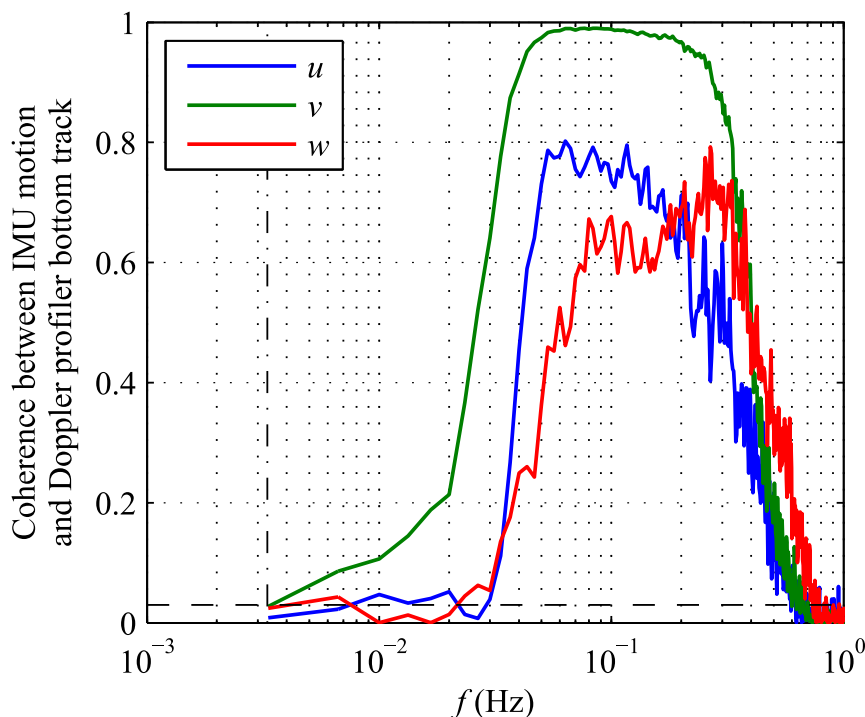


FIG. A1. Coherence between IMU-measured motion of SMB and ADCP-BT velocity for  $1.0 < U < 1.5 \text{ m s}^{-1}$ :  $u$  (blue),  $v$  (green), and  $w$  (red). The vertical dashed-dotted line indicates the frequency of the high-pass filter applied to the IMU accelerometers in estimating the motion of the ADV head. The horizontal dashed line indicates the 95% confidence level for the 102 spectral windows in this estimate.

Energy's Wind and Water Power Program (Contract DE-AC06-76RLO 1830).

The U.S. government retains and the publisher, by accepting the article for publication, acknowledges that the U.S. government retains a nonexclusive, paid-up, irrevocable, worldwide license to publish or reproduce the published form of this work, or allow others to do so, for U.S. government purposes.

## APPENDIX

### Combined Motion Spectra of ADV-IMU and ADCP-BT

The motion of the SMB platform was recorded using two methods of measurement: an IMU integrated with an ADV and the BT functionality of an ADCP.

The IMU motion is recorded at a relatively high frequency but is unable to capture low-frequency linear velocities due to the inherent signal drift of the integral of the measured acceleration, as described in Part II.

The bottom-tracking method of the ADCP calculates the platform motion using the Doppler shift of acoustic pulses reflected from the seabed. The sample frequency of this method is limited to the order of  $f = 2 \text{ Hz}$ , to avoid

signal contamination due to ringing in the transducer head. The BT measurements are compensated for rotation-induced motion using the orientation sensors of the instrument. As such, the ADCP-BT measurement represents the low-frequency motion of the SMB at the ADCP location.

To better understand the IMU's signal-to-noise ratio, the motion of the StableMoor buoy from the ADCP-BT measurements  $u_{\text{BT}}$  was compared to the IMU's estimates of ADP motion. To do this, the IMU's estimate of ADP motion was computed using the method described in section 3, using  $\mathbf{I}^*$  to describe the vector that points from the IMU to the ADCP head. In this case, we use a 5-min high-pass filter ( $f_a = 0.0033$ ) in Eq. (1) to reduce spectral reddening that otherwise contaminates coherence estimates while preserving the estimates of  $u_a$  at the frequencies where we wish to compare to the ADP bottom track. Clock offset and drift between the ADCP-BT and ADV-IMU datasets were identified using the peak cross correlation of the two signals. The ADCP clock began with an offset of 2.8 s and drifted by 0.07 s per hour relative to the ADV clock. The measurements of the ADCP-BT velocities were then synchronized and linearly interpolated onto the times of the ADV-IMU measurements.

The coherence between these two signals is high and statistically significant over 1.5 decades, from 0.03 to 0.8 Hz (Priestley 1981) as shown in Fig. A1. The  $v$  component has the highest coherence, 98%, because this is the direction that has the most motion (i.e., these estimates have a higher signal-to-noise ratio). The  $u$  and  $w$  components have a slightly lower coherence, 80% and 65%, respectively.

On the low-frequency side, the signal-to-noise ratio of the IMU decreases dramatically below 0.03 Hz, resulting in low coherence. On the high-frequency side, Doppler noise in the ADP measurements contaminates its estimates of motion, causing the decrease in coherence at 0.8 Hz. A comparison of the phase between these signals shows that there is no lag between the measurements (not shown). The rapid decrease in coherence below 0.03 Hz provides an objective measurement of the frequency at which IMU-measured velocity becomes unreliable in the flow conditions we observed.

#### REFERENCES

- Afgan, I., J. McNaughton, S. Rolfo, D. D. Apsley, T. Stallard, and P. Stansby, 2013: Turbulent flow and loading on a tidal stream turbine by LES and RANS. *Int. J. Heat Fluid Flow*, **43**, 96–108, doi:10.1016/j.ijheatfluidflow.2013.03.010.
- Govardhan, R. N., and C. H. K. Williamson, 2005: Vortex-induced vibrations of a sphere. *J. Fluid Mech.*, **531**, 11–47, doi:10.1017/S0022112005003757.
- Guerra París, M., and J. Thomson, 2017: Turbulence measurements from five-beam acoustic Doppler current profilers. *J. Atmos. Oceanic Technol.*, **34**, 1267–1284, doi:10.1175/JTECH-D-16-0148.1.
- Kilcher, L. F., J. Thomson, and J. Colby, 2014: Determining the spatial coherence of turbulence at MHK sites. *Proc. Second Marine Energy Technology Symp. (METS2014)*, Seattle, WA, Marine Energy Technology Symposium, 7 pp.
- , —, J. Talbert, and A. DeKlerk, 2016: Measuring turbulence from moored acoustic Doppler velocimeters: A manual to quantifying inflow at tidal energy sites. National Renewable Energy Laboratory Tech. Rep. NREL/TP-5000-62979, 34 pp.
- , —, S. F. Harding, and S. Nylund, 2017: Turbulence measurements from compliant moorings. Part II: Motion correction. *J. Atmos. Oceanic Technol.*, **34**, 1249–1266, doi:10.1175/JTECH-D-16-0213.1.
- Kraus, N. C., A. Lohrmann, and R. Cabrera, 1994: New acoustic meter for measuring 3D laboratory flows. *J. Hydraul. Eng.*, **120**, 406–412, doi:10.1061/(ASCE)0733-9429(1994)120:3(406).
- LORD MicroStrain, 2014: LORD datasheet: 3DM-GX3-25-OEM; OEM attitude heading reference system (AHRS). Doc. 8400-0030, Revision A, LORD Corporation, 2 pp.
- Matt, S., W. Hou, S. Woods, W. Goode, E. Jarosz, and A. Weidemann, 2014: A novel platform to study the effect of small-scale turbulent density fluctuations on underwater imaging in the ocean. *Methods Oceanogr.*, **11**, 39–58, doi:10.1016/j.mio.2015.01.001.
- Milne, I. A., A. H. Day, R. N. Sharma, and R. G. J. Flay, 2015: Blade loading on tidal turbines for uniform unsteady flow. *Renewable Energy*, **77**, 338–350, doi:10.1016/j.renene.2014.12.028.
- Moum, J. N., and J. D. Nash, 2009: Mixing measurements on an equatorial ocean mooring. *J. Atmos. Oceanic Technol.*, **26**, 317–336, doi:10.1175/2008JTECHO617.1.
- Nortek AS, 2005: Vector current meter. User Manual Doc. N300-100, Revision H, 86 pp.
- Paskyabi, M. B., and I. Fer, 2013: Turbulence measurements in shallow water from a subsurface moored moving platform. *Energy Procedia*, **35**, 307–316, doi:10.1016/j.egypro.2013.07.183.
- Perlin, A., and J. N. Moum, 2012: Comparison of thermal variance dissipation rates from moored and profiling instruments at the equator. *J. Atmos. Oceanic Technol.*, **29**, 1347–1362, doi:10.1175/JTECH-D-12-00019.1.
- Polagye, B., and J. Thomson, 2013: Tidal energy resource characterization: Methodology and field study in Admiralty Inlet, Puget Sound, WA (USA). *Proc. Inst. Mech. Eng.*, **227A**, 352–367, doi:10.1177/0957650912470081.
- Priestley, M., 1981: *Spectral Analysis and Time Series*. Probability and Mathematical Statistics, Vol. 2, Academic Press, 877 pp.
- Thomson, J., B. Polagye, V. Durgesh, and M. C. Richmond, 2012: Measurements of turbulence at two tidal energy sites in Puget Sound, WA. *IEEE J. Oceanic Eng.*, **37**, 363–374, doi:10.1109/JOE.2012.2191656.
- , L. F. Kilcher, M. Richmond, J. Talbert, A. DeKlerk, B. Polagye, M. Guerra, and R. Cienfuegos, 2013: Tidal turbulence spectra from a compliant mooring. *Proc. First Marine Energy Technology Symp. (METS2013)*, Washington, DC, Marine Energy Technology Symposium, 9 pp.
- , —, and S. Harding, 2014: Multi-scale coherent turbulence at tidal energy sites. *Proc. Fifth Int. Conf. on Ocean Energy (ICOE2014)*, Halifax, NS, Canada, Marine Renewables Canada, 6 pp. [Available online at [http://www.icoe2014canada.org/wp-content/uploads/2014/11/4-KilcherLevi\\_2-3web.pdf](http://www.icoe2014canada.org/wp-content/uploads/2014/11/4-KilcherLevi_2-3web.pdf).]
- Williamson, C. H. K., and R. Govardhan, 1997: Dynamics and forcing of a tethered sphere in a fluid flow. *J. Fluids Struct.*, **11**, 293–305, doi:10.1006/jfs.1996.0078.